Heparosan as a potential alternative to hyaluronic acid for the design of biopolymer-based nanovectors for anticancer therapy

Marlène Rippe, Talitha F Stefanello, Vanessa Kaplum, Elizandra A Britta, Francielle P Garcia, Robin Poirot, Mychelle V P Companhoni, Celso V Nakamura, Anna Szarpak-Jankowska, Rachel Auzély-Velty

ARTICLE

Heparosan as a potential alternative to hyaluronic acid for the design of biopolymer-based nanovectors for anticancer therapy

Received 00th January 20xx,
Accepted 00th January 20xx

DOI: 10.1039/x0xx00000x

www.rsc.org/

Marlène Rippe,[a] Talitha F. Stefanello,[b] Vanessa Kaplum,[b] Elizandra A. Britta,[b] Francielle P. Garcia,[b] Robin Poirot,[a] Mychelle V. P. Companhoni,[b] Celso V. Nakamura,[b] Anna Szarpak-Jankowska,[a] Rachel Auzély-Velty *[a]

Glycosaminoglycans (GAGs) are important components of the extracellular matrix that have attracted great interest for drug delivery and pharmaceutical applications due to their diverse biological functions. Among GAGs, heparosan (Hep), a biosynthetic precursor of heparin, has recently emerged as a promising building block for the design of nanoparticles with stealth properties. Though this non-sulfated polysaccharide has a chemical structure very close to that of hyaluronic acid (HA), it distinguishes from HA in that it is biologically inert in the extracellular spaces in the body. In this study, we designed Hep- and HA-based nanogels (NGs) that differ only in the chemical nature of the hydrophilic shell. The nanogels were prepared in a very straightforward way from Hep and HA modified with a thermoresponsive copolymer properly designed to induce self-assembly below room temperature. This versatile synthetic approach also enabled further shell-crosslinking allowing to increase colloidal stability. After careful characterization of the un-crosslinked and crosslinked Hep and HA NGs in terms of size (Z-average diameters of un-crosslinked and crosslinked NGs ~ 110 and 150 nm) and morphology, they were injected intravenously into tumor-bearing mice for biodistribution experiments. Interestingly, these show that the liver uptake of Hep nanogels is remarkably reduced and tumor accumulation significantly improved as compared to HA nanogels (intensity ratios of tumor-to-liver of 2.2 and 1.4 for the un-crosslinked and crosslinked Hep NGs versus 0.11 for the un-crosslinked and crosslinked HA ones). These results highlight the key role played by the shell-forming GAGs on the in vivo fate of nanogels, which correlates with the specific biological properties of Hep and HA.

Introduction

Self-assembled nanogels, nanometer-sized hydrogels obtained by physical self-assembly of interactive hydrophilic polymers, have attracted growing interest for drug delivery as these systems combine the advantages of hydrogels with nanoscale formulations.[1-5] These soft nanoparticles (NPs) can be designed to facilitate the encapsulation of diverse classes of bioactive compounds, and their hydrophilic shell can be exploited to control their biological behavior and targeting ability. In this regard, nanogels made of amphiphilic polysaccharides hold promise as versatile nanocarriers due to the presence of various functional groups on shell-forming polysaccharides in addition to their unique physicochemical properties, including biocompatibility and biodegradability.[1, 6] Among polysaccharides, glycosaminoglycans such as hyaluronic acid and chondroitin sulfate (CS) are being used increasingly to design self-assembled nanoparticles for tumor-targeted drug delivery.[7-16] These two GAGs can indeed be specifically recognized by cell surface CD44 receptors that are over-expressed by several cancer cells[17-20]. Yet, these polysaccharides also bind to other receptors in the human body, such HA receptor for endocytosis (HARE) that facilitates efficient receptor-mediated endocytosis[21, 22]. Moreover, CD44 and other variants are also expressed on a wide variety of normal cell types, including epithelial cells and haematopoietic cells.[23-26] In this regard, Bhattacharya et al. recently raised the question of exploiting HA-CD44 interactions to selectively deliver cytotoxic drugs to cancer cells,[27] observing the uptake of their HA-derived nanoparticles into CD44-expressing tumors and in other organs, i.e. liver and spleen[28, 29]. Based on this, they rationally modified HA through its *N*-deacetylation and selective sulfation to investigate the potential to minimize interaction of HA with CD44, with the aim of achieving maximum tumor accumulation.[27]

In this study, we explored the possibility of using heparosan as a potential alternative to HA for designing nanogels as drug carriers for tumor-targeted drug delivery. This was motivated by the "stealthty" properties of this GAG,[30-33] although its chemical structure is very similar to HA. Indeed, Hep has a repeating disaccharide unit of D-glucuronic acid (GlcA) and *N*-acetyl-D-glucosamine (GlcNAc) residues such as HA, but the α-1,4 bond between the GlcA and the GlcNAc units replaces the β-1,3 bond found in HA (Scheme 1). Moreover, since Hep is the natural precursor to the heparin/heparan sulfate biosynthesis, it is biocompatible. This non-sulfated GAG appears to be biologically inert in the extracellular spaces; indeed, it is not known to participate in biological binding interactions.[31] Moreover, it has no known extracellular degradation pathway and thus, it is stable in the bloodstream contrary to HA and heparin/heparan sulfate which are degraded by enzymes in the blood. On the other hand, Hep is degraded by lysosomal enzymes following entry into the

[a] Univ. Grenoble Alpes, Centre de Recherches sur les Macromolécules Végétales (CERMAV-CNRS), 601, rue de la Chimie, BP 53, 38041 Grenoble Cedex 9 (France)
* E-mail: rachel.auzely@cermav.cnrs.fr
[b] Laboratory of technological innovation in the development of pharmaceuticals and cosmetics, State University of Maringa, Colombo Avenue, 5790, 87020-900, Maringa, Brazil

Electronic Supplementary Information (ESI) available: [details of any supplementary information available should be included here]. See DOI: 10.1039/x0xx00000x

cell, which avoids accumulation in the body.[31] The peculiar features of Hep have recently attracted interest for its use as a potential alternative to poly(ethylene glycol) (PEG) in the design of nanocarriers for passive tumor targeting in anticancer therapy. Indeed, though the modification of nanoparticles with PEG is a widely adopted approach to extend blood circulation time and improve drug efficacy, several papers from the past decade have suggested that PEG can elicit antibody formation against PEG (anti-PEG) and can also trigger complement activation.[34-37] Therefore, to propose alternative stealth nanoparticles, some research teams developed NPs by the self-assembly of Hep modified with deoxycholic acid, cholesterol or the anticancer drug doxorubicin (DOX).[30, 32, 33, 38] These authors showed potential of these systems for intracellular delivery of DOX in vitro. Furthermore, incubation of heparosan-based drug delivery systems with different cancer cells revealed that these nanocarriers have different uptake and subcellular distribution behavior in tumor cells.[32] However, the in vivo behaviour of the nanocarriers was not investigated. Besides these self-assembled NPs, Hep-coated liposomes were also prepared by post-insertion of Hep-lipid conjugates.[39] Interestingly, these liposomes loaded with DOX were shown to impair tumor growth in a mouse breast cancer model similar to PEG-coated DOX-liposomes, supporting the idea of using Hep as a shell-forming polysaccharide of nanocarriers for anti-cancer therapy.

In this work, we designed Hep- and HA-based nanogels possessing similar properties in terms of chemical composition (except the hydrophilic shell), size and morphology to best assess the effect of the outer shell-forming GAG on their in vivo biodistribution and tumor-targeting efficiency after intravenous administration in Ehrlich solid tumor-bearing mice. The nanogels were prepared by temperature-induced self-assembly of Hep and HA suitably modified with a thermoresponsive ethylene glycol-based copolymer (Scheme 1). Such temperature-triggered approach allows spontaneous nanogel formation due to the dehydration of the grafted copolymer chains when heated above the cloud point temperature (T_{cp}). Herein, we synthesized a copolymer of di(ethylene glycol) methacrylate and butylmethacrylate (poly(DEGMA-co-BMA)) exhibiting a T_{cp} well below the room temperature by judiciously adjusting the comonomer ratio. This allowed obtaining stable nanogels at room temperature as required for good handling and biological application. Shell-crosslinked (SCL) nanogels were also designed to increase their colloidal stability (Scheme 1).

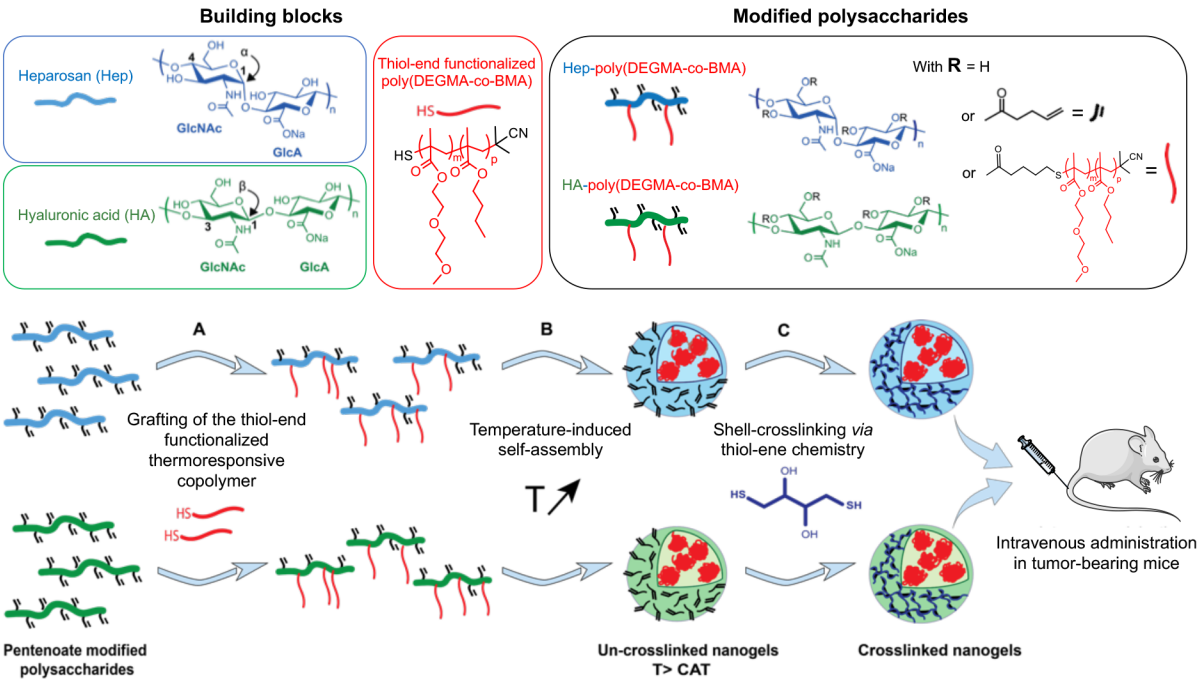

Scheme 1. Strategy for the synthesis of un-crosslinked and shell-crosslinked nanogels based on heparosan and hyaluronic acid modified with poly(DEGMA-co-BMA) (Hep-poly(DEGMA-co-BMA) and HA-poly(DEGMA-co-BMA)). A) Grafting of the thermoresponsive copolymer on Hep and HA using radical thiol-ene chemistry; B) formation of nanogels by temperature-triggered self-assembly of modified Hep and HA, and C) shell-crosslinking using radical thiol-ene chemistry.

They were prepared in a very straightforward way using thiol-ene chemistry[40, 41] allowing i) the coupling of the thiol-end functionalized copolymer with the polysaccharide modified with alkene groups and, ii) the subsequent crosslinking of the shell-forming polysaccharide by reaction of a bi-functional thiol reagent with the remaining alkene groups. The Hep and HA nanogels were then carefully characterized in terms of size, morphology and cytotoxicity. Finally, their in vivo biodistribution was evaluated by near-infrared fluorescence imaging to shed some light on the role of GAGs on the in vivo fate of the nanogels. To our knowledge, this study provides the first comparison of the in vivo behavior of HA and Hep-based nanoparticles that differ only in the hydrophilic outer shell.

Materials and methods

Materials

Hyaluronic acid samples (M_w = 20 and 40 kg/mol) were purchased from Lifecore (USA). Heparosan (M_w = 30 kg/mol) was kindly provided by HTL (Javené, France). (Diethylene glycol) methyl ether methacrylate, butyl methacrylate, 2-cyano-2-propyl benzodithioate, 2,2-azobis(2-methylpropionitrile), phosphate buffer saline (PBS, pH 7.4), sodium chloride, aluminum oxide, tris-(2-carboxyethyl) phosphine hydrochloride (TCEP), *n*-butylamine, 4-pentenoic anhydride, thiazolyl blue tetrazolium bromide, 1,4-dithiothreitol and 4-(4,6-dimethoxy-1,3,5-triazin-2-yl)-4-methylmorpholinium chloride were purchased from Sigma-Aldrich-Fluka (France). 2-Hydroxy-1-[4-(2-hydroxy-ethoxy)phenyl]-2-methyl-1-propanone (Irgacure 2959) was kindly provided by Ciba Speciality Chemicals (Basel, Switzerland). Sulfo-Cyanine7 amine (Cy7-amine) was purchased from Lumiprobe. Dulbecco's Modified Eagle's Medium (DMEM), L-glutamine and fetal bovine serum (FBS) were provided by Gibco. All chemicals, except DEGMA and BMA which were purified by running them through a column packed with aluminum oxide, were used without any further purification. The positively charged resin, diethylaminoethyl cellulose (DEAE Sepharose CL-6B) was purchased from GE Healthcare Life Science. Spectra/Por 1 (MWCO 6-8000 g/mol) membrane used for dialysis was obtained from Fisher Scientific (Rancho Domingez, CA). The water used in all experiments was purified by a Elga Purelab purification system, with a resistivity of 18.2 MΩ cm. Deuterium oxide (D_2O) and deuterated dichloromethane ($CDCl_3$) were obtained from SDS (Vitry, France).

Analytical techniques

^{1}H NMR spectra were recorded at 5, 25 or 80 °C using a Bruker AVANCE III HD spectrometer operating at 400 MHz. All spectra were recorded by applying a 45° tip angle for the excitation pulse, and a 10 s recycle delay. Chemical shifts (δ in ppm) are given relative to external tetramethylsilane (TMS = 0 ppm) and calibration was performed using the signal of the residual protons of the solvent as a secondary reference. Fourier transform infrared spectroscopy (FTIR) measurements were performed on a RX1 spectrometer (Perkin Elmer, UK) with horizontal ATR accessory. For each sample, 32 scans were recorded between 4000 and 400 cm^{-1} with a resolution of 2 cm^{-1} using the Spectrum software V 5.0.0. The spectra was then analyzed using the Origin 7.0 software. The number-average molar mass (M_n), the weight-average molar mass (M_w) and the dispersity (*Đ*) of poly(DEGMA-co-BMA) were determined by size exclusion chromatography (SEC) in dimethylformamide containing 50 mM $NaNO_3$. Measurements were done on a GPC system equipped with a Waters model 515 pump, a refractive Index Detector RI 2000 from Schambeck SFD GmbH and a light scattering detector (MALLS) from Wyatt (USA). The samples were analysed using a 161123-Agilent-10 column at 30 °C and at a flow rate of 1 mL/min. The cloud point temperature (T_{cp}) of poly(DEGMA-co-BMA) was determined by UV-vis turbidity measurements (λ = 500 nm) performed on a Varian Cary 50 Scan. The samples were prepared at 4 °C in PBS (0.5 g/L), after which the sample was placed in the instrument. The light transmittance was measured during at least two controlled cooling/heating cycles from 10 °C to 40 °C using a 1°C/10 min interval. T_{cp} was considered to be the temperature at which the light transmittance was 50 % of that obtained for the same sample at 10 °C. The critical aggregation temperature (CAT) of HA-poly(DEGMA-co-BMA) or Hep-poly(DEGMA-co-BMA) in aqueous solution was assessed using a Zetasizer NanoZS Malvern Instruments apparatus equipped with a HeNe laser at 173° and a temperature controller. A solution of HA-poly(DEGMA-co-BMA) or Hep-poly(DEGMA-co-BMA) in PBS at a concentration of 0.5 mg/mL was filtered through a 0.45 µm polycarbonate filter and heated from 10 to 40 °C using a 5 °C interval. The CAT was considered to be the temperature at the intersection between the lower horizontal portion of the plotted curve (average scattered intensity versus temperature dependence) and the tangent line of the curve. The size and size distribution of nanogels were simultaneously measured with the CAT by dynamic light scattering (DLS) using a Zetasizer NanoZS Malvern Instruments apparatus operating with a HeNe laser at 173°. The hydrodynamic diameters were calculated from diffusion coefficients using the Stokes-Einstein equation. All correlogram analyses were performed with software supplied by the manufacturer. All the measurements were performed in PBS (pH 7.4, [NaCl] = 0.15 M).

Synthesis of poly(DEGMA-co-BMA)

DEGMA (10 g, 50 mmol) and BMA (0.398 g, 2.79 mmol), the RAFT agent 2-Cyano-2-propyl benzodithioate (0.082 g, 0.372 mmol) and AIBN (3 mg, 0.0186 mmol) in anhydrous toluene (25 mL) were placed in a round bottom Schlenk flask and oxygen was removed via bubbling the mixture under nitrogen atmosphere for 30 min. Then, the flask was sealed and placed in a thermostatic oil bath pre-heated at 80 °C. The reaction was quenched by cooling and exposure to oxygen. The resulting copolymer was precipitated in cyclohexane. The precipitate was dissolved in dichloromethane and the copolymer was precipitated again in cyclohexane. The resulting precipitate was finally dried under high vacuum to give 6 g of pure poly(DEGMA-co-BMA). Samples taken before and during the polymerization were analyzed by ^{1}H NMR to determine monomers conversion. The M_n, M_w and *Đ* values of the copolymer were determined by size exclusion chromatography in DMF.

Synthesis of HA-poly(DEGMA-co-BMA) and Hep-poly(DEGMA-co-BMA)

The pentenoate modified HA20 (M_w = 20 kg/mol) and Hep30 (M_w = 30 kg/mol) derivatives with a degree of substitution of 0.5 were synthesized as previously described.[41] The poly(DEGMA-co-BMA) copolymer was subjected to aminolysis using *n*-butylamine, to convert the RAFT end-group to a thiol. Briefly, the copolymer (600 mg, 0.375 mmol) was solubilized in dichloromethane (9 mL) and *n*-butylamine (6.5 mL, 66 mmol) was added. After 5 min under stirring at room temperature, the reaction mixture was concentrated under reduced pressure, resulting in a waxy liquid that was solubilized in dichloromethane. The copolymer was recovered by precipitation in cyclohexane and dried under vacuum at 45 °C during 4 hours to remove residual solvent. Next, the thiol-end-functionalized copolymer (550 mg, 0.0312 mmol) was solubilized in 14 mL of pure water and TCEP (10 mg, 0.0350 mmol) was added. After 30 min of

stirring at 4 °C under nitrogen atmosphere, the copolymer solution was added to an aqueous solution of pentenoate modified HA or pentenoate modified Hep (50 mg, 0.116 mmol) in pure water (4 mL), followed by a solution of Irgacure 2959 (2 mL) in water (10 g/L) in order to obtain a final photoiniator concentration of 0.1 % (w/v) in the reaction media. The reaction mixture cooled in a ice bath, was exposed to UV light (λ = 365 nm) with an intensity of 20 mW/cm^2 for 5 min under stirring and nitrogen atmosphere. The resulting HA-poly(DEGMA-co-BMA) and Hep-poly(DEGMA-co-BMA) derivatives were purified via a batch ion exchange process using DEAE Sepharose CL-6B as a weak-anion exchanger. Briefly, DEAE resin (20 mL), stored in a solution of ethanol 30 %, was washed three times with ultrapure water at 4 °C (3 × 20 mL, contact times of 10 min). Excess liquid was removed by centrifugation (10000 rpm, 10 min) at 4° C. Then, the resin was activated by successive washes with a 0.5 M NaCl aqueous solution (20 mL), a 1 M NaCl aqueous solution (20 mL) and finally, four times with ultrapure water (4 × 20 mL). The HA-poly(DEGMA-co-BMA) or Hep-poly(DEGMA-co-BMA) derivative was then added to the resin in a conical tube and allowed to interact with the resin overnight at 4°C under stirring with an orbital shaker. Then, the HA or Hep derivative bound to the resin was subjected to seven washes with ultrapure water (7 × 20 mL) to remove un-grafted copolymer. Finally, the HA or Hep derivative was eluted with a 1 M NaCl aqueous solution (4 × 10 mL). After filtration of the solutions of the HA or Hep derivative through a Buchner funnel with a porous glass filter plate (porosity 4), the solution was dialyzed against deionized water (membrane with cut-off 6-8 Da MW, 72 h). The product was recovered by freeze-drying as a white powder.

Synthesis of crosslinked nanogels

To a solution of HA-poly(DEGMA-co-BMA) or Hep-poly(DEGMA-co-BMA) (0.015 g, 0.022 mmol) with a DS of 0.03 at a concentration of 0.5 g/L in PBS (pH 7.4) at 4°C under nitrogen atmosphere in an ice bath, 564 µL (1.41 mg, 0.009 mmol) of a solution of DTT in PBS (2.5 g/L) was added under stirring. Next, the temperature of the solution was increased to 40°C (above the CAT). After stirring at 40°C for 45 min, 3.3 mL of an aqueous solution of Irgacure 2959 (10 mg/mL) was then added to the nanogels suspension to obtain a final photoiniator concentration of 10 % (w/v). The mixture was exposed to UV light (λ = 365 nm) with an intensity of 20 mW/cm^2 for 15 min under stirring and nitrogen atmosphere. The nanogels suspension was transferred into a dialysis bag (MWCO = 6-8000 g/mol) and dialyzed against deionized water for 72 h. The shell cross-linked nanogels were recovered by freeze-drying. The volume of the DTT solution (218 µL, 652 µL) was varied to obtain [SH]/[=] ratios of 1 and 2, respectively. Next, the temperature of the solution was increased to 40 °C.

Determination of the degree of substitution of HA-poly(DEGMA-co-BMA) and Hep-poly(DEGMA-co-BMA) samples by the carbazole reaction

The DS was indirectly determined by reaction of D-glucuronic acid units of HA with carbazole [26] Briefly, 800 µL of 25 mM sodium tetraborate solution in sulfuric acid was added to an aqueous solution of HA-poly(DEGMA-co-BMA) or Hep-poly(DEGMA-co-BMA) (200 µL) at a concentration of 0.1 g/L. After heating at 100 °C for 10 min, the solution was cooled at room temperature for 15 min, and then a solution of carbazole (200 µL) in absolute ethanol 0.125 % (m/v) was added. The sample was heated again at 100 °C for 10 min and its absorbance was determined by spectrophotometry at 530 nm. The polysaccharide concentration was calculated from a calibration curve (0.050 to 0.200 g/L), which allowed the indirect determination of copolymer amount in the HA- and Hep-poly(DEGMA-co-BMA) samples.

Scanning electron microscopy and transmission electron microscopy

For SEM analysis, drops of un-crosslinked and crosslinked nanogels solutions (0.5 mg/mL) in ultrapure water at both 5 and 40 °C were deposited onto mica-coated copper stubs (also precooled/heated at 5 or 40 °C, respectively) and allowed to air drying at 5 or 40 °C. The samples were then coated by approximately 2 nm of sputtered Au-Pd and observed in secondary electron imaging mode with a ZEISS Ultra 55 FEG-SEM (Grenoble INP - CMTC). Images were acquired at low voltage of 3 kV using an in-lens detector. For TEM analysis, all samples were dispersed in ultrapure water, stained with 5 % uranyl acetate and observed with a JEOL JEM 1400 (Jeol, USA) transmission electron microscope operating at 120 kV acceleration voltage.

Labeling of nanogels based on HA-poly(DEGMA-co-BMA) and Hep-poly(DEGMA-co-BMA) with sulfo-cyanine7

Fluorescent nanogels were prepared by grafting the dye Cy7-amine on un-crosslinked and crosslinked nanogels based on HA-poly(DEGMA-co-BMA) and Hep-poly(DEGMA-co-BMA) by an amine-acid coupling reaction using DMTMM as a coupling agent[42]. To this end, crosslinked nanogels (0.008g, 0.0135 mmol) were solubilized in water/DMF (1:1 v/v; 4 mL) and DMTMM (3.7 mg, 0.0135 mmol) was added to the solution, followed by adjusting the pH to 6.5. After 30 min of stirring, Cy7-amine (0.5 mg, 0.000676 mmol) solubilized in water/DMF (1:1 v/v) at a concentration of 5 g/L was added to the reaction mixture. After stirring at room temperature for **72 h**, the nanogels were purified by dialysis using a membrane MWCO 6-8 kg/mol against a mixture of water/ethanol (2/1 v/v) then, against deionized water for 48 h and finally, they were recovered by freeze-drying.

Cytotoxicity assay

Vero cells (ATCC, Maryland) were maintained in DMEM supplemented with 2 mM L-glutamine and 10% heat-inactivated FBS at 37 °C in a 5% CO_2 atmosphere. In order to investigate a possible toxicity of Hep and HA nanogels towards mammalian cells, Vero cells obtained from confluent cultures were plated (5 x 10^5 cells/mL) in 96-well plates and incubated for 24 h at 37 °C in a 5% CO_2 atmosphere. Next, the cells were treated with different concentrations (10 – 1000 µg/mL) of HA and Hep NGs as well as the native polysaccharides solutions in DMEM. After 72 h of incubation, the cultures were evaluated by MTT assay, as previously described[43]. After treatment, the medium was removed, and the cellular

monolayer was washed with 0.01 M PBS (pH 7.4), and 50 µL of MTT solution at 2 mg/mL were added to each well. After incubation for 4 h at 37 °C protected from light, MTT solution was removed and 150 µL of DMSO was added to each well. Absorbance was read in a microplate reader (BIO-TEK Power Wave XS) at 570 nm. The percentage of viable cells was calculated compared with controls (not treated cells). The concentration that decreased 50% of the absorbance compared with the control cells was considered the toxic concentration for 50% of cells (CC_{50}).

In vivo biodistribution

All in vivo procedures were carried out in accordance with the Brazilian legislation issued by the National Council for Control of Animal Experimentation (CONCEA) and was approved by the Ethic Committee on Animal Use of State University of Maringá (CEUA/UEM), protocol number CEUA 6160200416. Male hairless mice (3 weeks old, 20-30 g, Brazil) were housed under controlled conditions of temperature (22 ± 1°C) and humidity, 12:12 h light/dark cycle and *ad libitum* access to food and water. Solid tumors were obtained by subcutaneously injecting a suspension of 1×10^7 Ehrlich ascites carcinoma (EAC) cells/mL in PBS (50 µL) on the right flanks of mice. After tumor grown period (≈10 days), animals were anesthetized with isoflurane 2% in an air/O_2 mixture, and 100 µL of suspensions of Cy7-labeled uncrosslinked and crosslinked HA and Hep NGs (3 g/L in PBS) were administered in the tail vein. For comparison, Cy7-labeled HA (M_w = 20 and 40 kg/mol) and Hep (M_w = 30, 3 g/L in PBS) were also injected. Immediately after injection, mice were evaluated using an In-vivo MS FX PRO (Carestream Molecular Imaging, Carestream Health, United States). Fluorescent images (λ exc = 750 nm; λ em = 790 nm) were obtained with a CCD camera (Kodak Image Station) at 0, 1, 3 and 24 h post-injection. Mice were then sacrificed and the main organs (liver, spleen, lung, kidney, heart, bladder and tumor) were removed for *ex-vivo* imaging. Images acquisition and semi-quantification of relative fluorescence intensity in regions of interest (ROI) were performed using Carestream Molecular Imaging 5.0 software (Carestream Molecular Imaging, Carestream Health, United States).

Results and discussion

Synthesis of poly(DEGMA-co-BMA)

The copolymer poly(DEGMA-co-BMA) was prepared *via* the reversible addition–fragmentation chain transfer (RAFT) process from di(ethylene glycol) methacrylate (DEGMA) and butylmethacrylate (BMA) monomers using 2,2-azobis(2-methylpropionitrile) (AIBN) as an initiator and 2-cyano-2-propyl benzodithioate (CPB) as a chain transfer agent (CTA) (Scheme 2A). A DEGMA/BMA ratio of 95:5 was selected to obtain a copolymer exhibiting a T_{cp} well below the room temperature and thereby, allowing formation of nanogels at room temperature (i.e. ~ 25 °C). ^{1}H NMR analysis was conducted to monitor the copolymerization kinetics. The kinetic plots proved that, in these reaction conditions, CPB allowed a good control over the RAFT copolymerization of DEGMA and BMA (Figure S1).

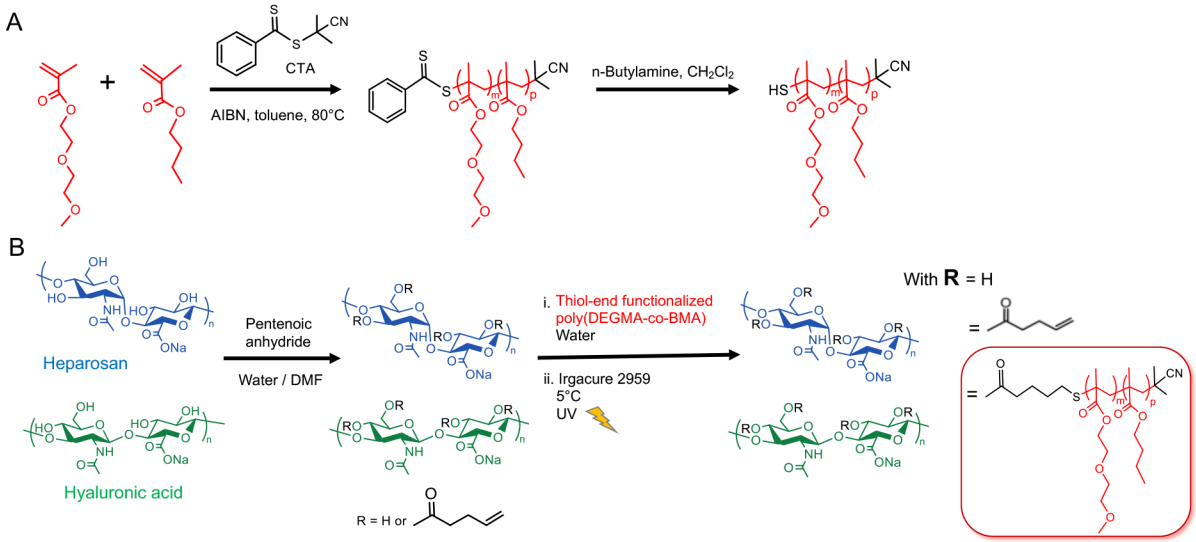

Scheme 2. Synthetic pathway to Hep- and HA-poly(DEGMA-co-BMA). A) Synthesis of poly(DEGMA-co-BMA) via the RAFT process; B) Grafting of the thermoresponsive copolymer on Hep and HA using radical thiol-ene chemistry

^{1}H NMR and size exclusion chromatography (SEC) analysis of the final copolymer revealed a final copolymer composition DEGMA/BMA of 95:5, a low dispersity ($Đ$ = 1.12), and a number average molar mass M_n of ~ 16 kg/mol ($M_{n,NMR}$ = 15500 g/mol, $M_{n,SEC}$ = 15740 g/mol, Figure S2). The copolymer exhibited a T_{cp} of 18 °C at 0.5 g/L in phosphate buffer saline (PBS), pH 7.4 (Figure S3).

Synthesis of HA and Hep-based nanogels

In order to couple poly(DEGMA-co-BMA) to HA and Hep, the polysaccharides were first esterified with pentenoic anhydride to produce ene-functional derivatives that were previously shown to react efficiently with various thiol-containing molecules via thiol–ene photochemistry.[40,41] The pentenoate modified HA and Hep (HA-p and Hep-p, respectively), possessing a degree of substitution (DS, average number of substituents per repeating unit) of 0.5, were subsequently reacted with poly(DEGMA-co-BMA) on which the RAFT end-group was converted to a thiol by aminolysis using *n*-butylamine (Scheme 2). The thiol-ene coupling reaction was conducted under UV-light irradiation (λ = 365 nm) in water, in the presence of Irgacure 2959 as a photoiniator. The HA- and Hep-poly(DEGMA-co-BMA) conjugates were then purified *via* a batch ion exchange process performed at low temperature (< 10 °C) to ensure effective removal of the non-grafted copolymer during washes with water, followed by a rapid dialysis to remove salt. This purification process, completed in less than four days, afforded the final products in 50 % yield. Successful grafting of the copolymer was confirmed by ^{1}H-NMR analysis. In the ^{1}H-NMR spectrum, the proton signals at 4.25 ppm, 3.76 ppm, 3.39 ppm and in the region of 0.99-1.2 ppm arising from poly(DEGMA-co-BMA) can easily be observed (Figure 1). The DS of the conjugates, determined by the carbazole assay,[44] were found to be 0.02 ± 0.01 for the HA- and Hep-poly(DEGMA-co-BMA) conjugates.

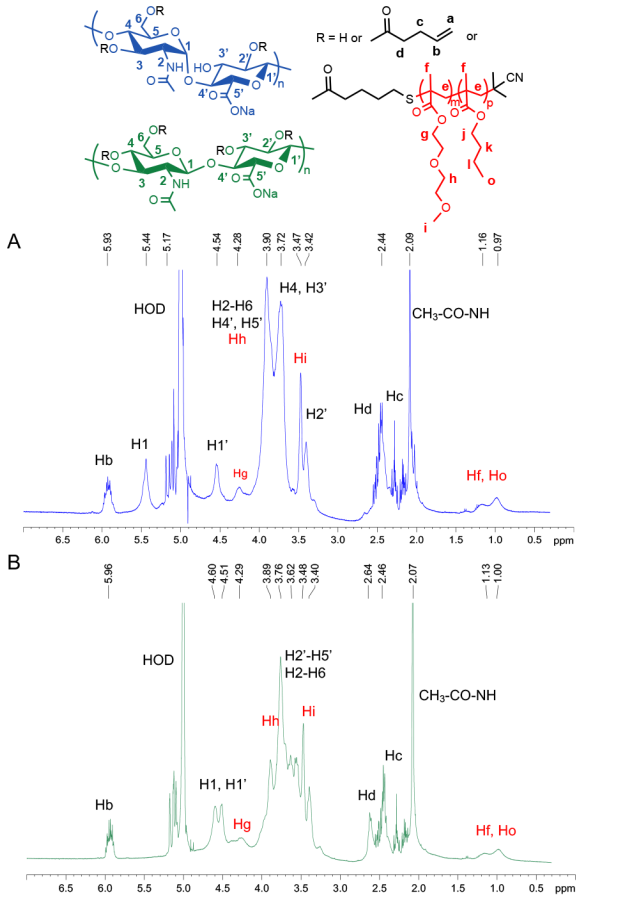

Figure 1. ^{1}H NMR spectra (400 MHz, 6 mg/mL in D_2O) of Hep-poly(DEGMA-co-BMA) (A) and HA-poly(DEGMA-co-BMA) (B) at 5°C.

Temperature responsiveness of Hep- and HA-poly(DEGMA-co-BMA)

Dynamic light scattering analysis of solutions of Hep- and HA-poly(DEGMA-co-BMA) in PBS at 37 °C revealed a monomodal size distribution for both derivatives, indicating their self-assembly into nanogels at the body temperature (Figure 2A). The Hep and HA-based nanogels exhibited a similar average size (mean diameter derived from the intensity distribution (D_h) ~115 nm and Z-Ave ~ 110 nm). The self-assembled gel nanoparticles of poly(DEGMA-co-BMA)-modified Hep and HA prepared in pure water were also observed by transmission electron microscopy (TEM) after drying at at 40°C (Fig. 2B).

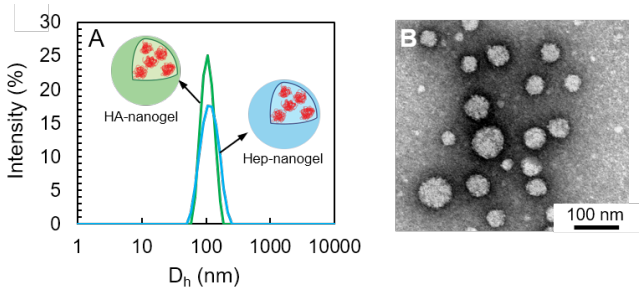

Figure 2. Temperature responsiveness of Hep- and HA-poly(DEGMA-co-BMA). A) Dynamic light scattering analysis of Hep and HA-poly(DEGMA-co-BMA) solutions in PBS (C_p = 0.5 g/L) at 37 °C. B) TEM image of Hep NGs in water at 40 °C (C_p = 0.5 g/L).

The critical aggregation temperature (CAT) of the HA- and Hep-poly(DEGMA-co-BMA) conjugates was determined by measuring the light scattering intensity (LSI) of aqueous solutions of the derivatives as a function of temperature (Figure 3). The CAT, defined as the temperature at the intersection between the lower horizontal portion of the plotted curve and the tangent line, was found to be 20 °C and 22 °C for HA- and Hep-poly(DEGMA-co-BMA), respectively. Both HA and Hep derivatives are thus able to self-assemble into nanogels at room temperature.

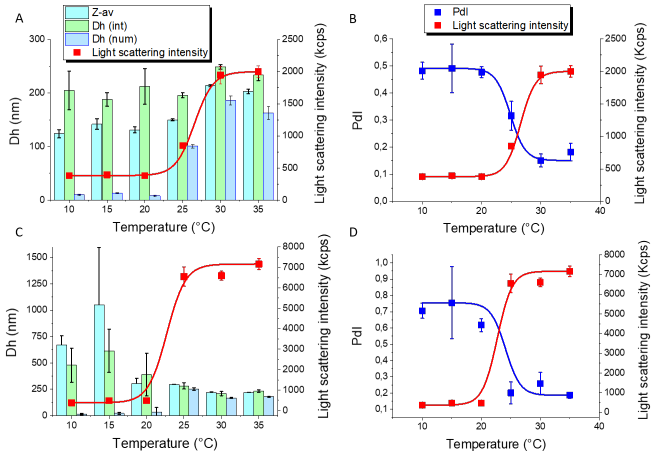

Figure 3. Analysis by DLS of the temperature sensitivity of Hep-poly(DEGMA-co-BMA) (A, B) and HA-poly(DEGMA-co-BMA) (C, D) in PBS (pH 7.4, C_p = 0.5 g/L). A and C) Variation of the D_h, Z-Ave and LSI values upon cooling from 35 °C to 10 °C (0.5 °C/min). B and D) Variation of the LSI and PdI upon cooling from 35 °C to 10 °C.

Self-assembly into well-defined nanostructures is also reflected in the sharp decrease of the polydispersity index (PdI) above the CAT as well as in the values of mean diameter in different distributions (intensity and number distribution) and of Z-average size, which are similar. In contrast, strong discrepancies between the mean size values are observed below the CAT.

Synthesis and characterization of shell-crosslinked nanogels

In order to avoid a fast destabilization of the nanogels structure after intravenous administration due to dilution of the polymers solution in the blood or by the interaction with blood components, the polysaccharide shell of Hep and HA NGs was crosslinked using thiol-ene chemistry by reaction of the remaining pentenoate groups with dithiothreitol (DTT) as a bis-thiol crosslinker (Figure 4A). This crosslinking step was performed under relatively dilute conditions (C_p = 0.5 g/L) to avoid inter-nanogel coupling, and by varying the [SH]/[=] ratio from 1 to 2 to ensure that all nanogels were sufficiently crosslinked to be stable at low temperature. Comparison of ^{1}H NMR spectra before and after the thiol-ene reaction with DTT provided evidence of successful shell-crosslinking (Figure 4B). Indeed, the addition of thiols to alkenes during the crosslinking step leads to the formation of thioether bonds and concomitantly, to the disappearance of the double bonds of the pentenoate groups. Consequently, the intensity of the alkene protons at 5.9 and 5.1-5.2 ppm is decreased and the signals of the methylene protons of the pentenoate groups at 2.1-2.3 ppm undergo a chemical shift. Furthermore, the proton signals of the polysaccharide backbone and the copolymer are significantly broadened since the crosslinking reaction decreases the mobility of the polymer chains.

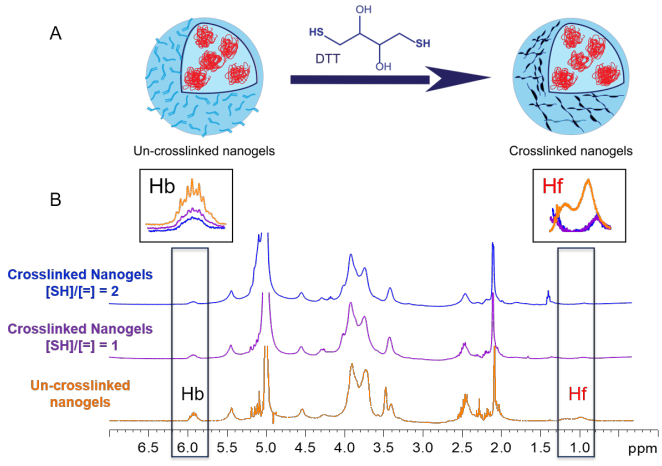

Figure 4. Shell crosslinking of NGs by reaction between DTT and alkene groups of the shell-forming polysaccharide. A) Reaction conditions: Irgacure 2959, UV-light (λ = 365 nm) exposure for 15 min, C_p = 0.5 g/L in PBS. B) Comparison of ^{1}H NMR spectra of un-crosslinked Hep NGs and crosslinked Hep NGs by varying the [SH]/[=] ratio from 1 to 2. The signal intensities were normalized relative to the intensity of the CH_3CO signal of HA

Successful crosslinking was further confirmed by FT-IR spectroscopy (Figure S4). In the IR spectra of the crosslinked nanogels, additional bands at 839 cm^{-1} and 911 cm^{-1} are observed after reaction with DTT, which can be attributed to C-S bend, C-S stretching and H-C-S bend, respectively. The new band observed at 1253 cm^{-1} (CH_2 vibrations) also suggests incorporation of DTT.[19-20]

Temperature responsiveness of crosslinked nanogels

While the un-crosslinked nanogels of Hep-p-poly(DEGMA-co-BMA) and HA-p-poly(DEGMA-co-BMA) disassemble below the CAT (~ 22 °C), their counterparts crosslinked with excess DTT ([SH]/[=] of 2) were found to be stable below the CAT. This was clearly demonstrated by DLS measurements at temperatures varying from 30 to 10 °C with a cooling rate of 0.3 °C/min (Figure 5). The LSI and PdI of the nanogels were constant upon cooling, demonstrating efficient nanogel crosslinking. Furthermore, scanning electron microscopy (SEM) images revealed the presence of nanogels at 5 °C (Figure 5C and 5F). It should be noted that a ratio of [SH]/[=] of 2 is required to ensure complete stability of nanogels. Indeed, the LSI of the nanogels crosslinked with a [SH]/[=] ratio of 1 slightly decreased upon cooling, suggesting dissociation of some nanogels (Figure S5).

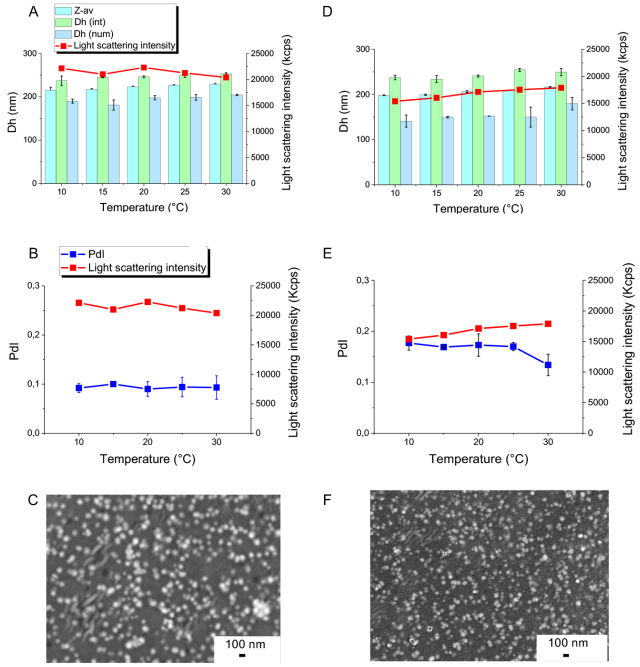

Figure 5. Analysis by DLS and SEM of crosslinked Hep NGs (A, B, C) and HA NGs (D, E, F) in PBS (pH 7.4, Cp = 0.5 g/L). A and D) Variation of the D_h, Z-Ave and LSI values upon cooling from 35 °C to 10 °C (0.3 °C/min). B and E) Variation of the LSI and PdI upon cooling from 35 °C to 10 °C. C and F) SEM observation at 5 °C.

Interestingly, the SCL nanogels showed temperature-dependent swelling/deswelling transitions between 15 and 40 °C. The swelling-deswelling transition was fully reversible over multiple heating/cooling cycles.

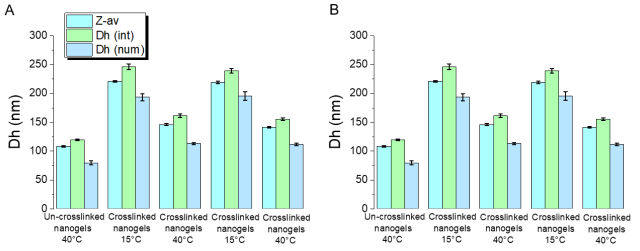

Figure 6. Analysis by DLS of the swelling-deswelling transition of crosslinked Hep-NGs (A) and HA-NGs (B) over multiple heating/cooling cycles (C_p = 0.5 g/L in PBS).

In vitro cytotoxicity, in vivo biodistribution and tumor targeting of crosslinked and uncrosslinked Hep-NGs and HA-NGs

The in vitro cytotoxicity of un-crosslinked and shell-crosslinked Hep NGs and HA NGs, as well as of native HA and Hep, was evaluated in Vero cells after 72 h of incubation by MTT assay. For all the samples, the toxic concentration for 50 % of the cells was higher than 1000 µg/mL, the maximum assessed concentration, demonstrating the very low cytotoxicity and biocompatibility of our HA and Hep derivatives (Figure S6).

The in vivo biodistribution and tumor targeting of Hep- and HA-based nanogels were then evaluated in Ehrlich solid tumor (EST)-bearing mice[45] by a non-invasive fluorescence imaging system. The main characteristics of the nanogels in terms of mean size and PdI near body temperature are summarized in Table 1. Importantly, the similar size of both HA- and Hep-based un-crosslinked nanogels as well as of both crosslinked ones together with their similar chemical composition, except the hydrophilic shell structure, allowed a proper comparison of the biodistribution of HA- and Hep NGs. The nanogels and the native polysaccharides, HA (M_w = 20 and 40 kg/mol) and Hep (M_w = 30 kg/mol), were labeled with the NIR dye Sulfo-Cyanine7 (Cy7) to visualize their biodistribution. Briefly, the samples were chemically modified with Cy7-amine using 4-(4,6-dimethoxy-1,3,5-triazin-2-yl)-4-methylmorpholinium chloride as an amine-acid coupling agent.[46] The content of Cy7 molecules in the polysaccharide derivatives (DS) was 0.002, as determined by UV/Vis spectroscopy at 680 nm. After Cy7 labeling, the nanogels maintained their size as shown by nanoparticle tracking analysis (NTA),[47] which enables the visualization and recording of nanoparticles in solution (Figure S7). Particle size distribution obtained by NTA ranged from 60 to 250 with an average of 150 ± 40 nm and from 60 to 300 with an average of 190 ± 43 nm for the SCL NGs based on HA and Hep, respectively (Figure S7).

Table 1. Size and polydispersity of nanogels based on Hep-poly(DEGMA-co-BMA) and HA-poly(DEGMA-co-BMA) determined by dynamic light scattering at 40 °C (0.5 g/L in PBS).

	Nanogels	Z-Average size (nm)	PdI
HA	Un-crosslinked nanogels	108 ± 1	0.174 ± 0.03
	Crosslinked nanogels (1 eq DTT)	151 ± 2	0.176 ± 0.01
Hep	Un-crosslinked nanogels	119 ± 1	0.095 ± 0.006
	Crosslinked nanogels (1 eq DTT)	146 ± 2	0.095 ± 0.013

Time-dependent biodistribution of Cy7-labeled native Hep, HA and nanogels on EST-bearing mice was observed after intravenous administration. Ex vivo fluorescence images of excised organs and tumors showed a higher accumulation of Hep NGs in the tumor than HA NGs. As shown in Figure 7A, the intensity ratio of tumor-to-liver between 1 h and 24 h was in the order un-crosslinked Hep NGs > crosslinked Hep NGs > un-crosslinked HA NGs ≈ crosslinked HA NG, suggesting lower liver uptake and higher tumor accumulation for the nanogels based on Hep. These results were consistent with those obtained from native polysaccharides (Figure 7B). Indeed, as can be seen from Figure 7B, the intensity ratio of tumor-to-liver is much higher for Hep (M_w = 30 kg/mol) than HA, whatever the molar mass of HA (20 or 40 kg/mol). Interestingly, the intensity ratio of tumor-to-liver for the Hep-NGs and native Hep progressively increased during the whole period of time studied (24 h).

The higher intensity ratio of tumor-to-liver at 24 h post-injection for the Hep NGs and native Hep in comparison to the HA NGs and native HA correlates with their very low liver uptake and significant tumor accumulation (Figure 7C-F). Notably, the ex vivo fluorescence images of the main organs displayed in Figure 7E clearly show that the liver uptake of nanogels based on Hep is remarkably reduced and tumor accumulation significantly improved. These results highlight the key role played by the shell-forming GAG on the in vivo fate of nanogels, taking into account the fact that the HA and Hep NGs are similar in terms of size and morphology. Regarding the in vivo behavior of the HA NGs, several research teams previously observed accumulation of HA-based nanoparticles and drug conjugates in the liver in addition to the uptake in the tumor.[28, 29, 48-52] This was found to be also the case with HA NPs administered in EST-bearing mice model, which is a well-established animal model for CD44 receptor overexpressing tumors.[45, 53-55] Two possible reasons for such accumulation in the liver were raised: cellular uptake by phagocytic cells of the reticuloendothelial system (RES) and interaction of HA with the HARE receptor which is expressed by liver sinusoidal endothelial cells and mediates systemic clearance of HA[21, 56]. Here, the fact that Hep NGs and native Hep are not sequestered by the liver rules out the idea that the hepatic accumulation of HA NGs and native HA is mainly due to non-specific uptake by phagocytic cells of the RES. Moreover, it is worth noting that a similar liver uptake was also observed for native unconjugated HA after intravenous administration in healthy mice, while native Hep did not accumulate in major organs (Figure S8). The preferential accumulation of native HA in the liver of healthy mice was previously reported by other research groups.[57-59] These data support the notion that the liver is the major site of circulating HA uptake and degradation in contrast to Hep which does not bind to HARE[21]. Actually, Hep stands out among other GAGs (HA, CS, heparin, dermatan sulfate) that selectively interact with HARE, resulting in their clearance from circulating lymph and blood.[21] This unique feature of Hep may be related to the fact this GAG is only temporarily present in the organism as it is the biosynthetic precursor of heparin and heparan sulfate. Therefore, as Hep is biologically inert in the extracellular environment, it can circulate in the bloodstream for a prolonged period of time. In this regard, it was previously reported that its half-life can vary from 15 h to 2 days depending on its molar mass (60 or 100 kg/mol).[60] As a result, the prolonged circulation of Hep in the bloodstream may increase its probability of reaching the tumor tissue after systemic administration in vivo as well as that of Hep NGs.

Finally, comparison of un-crosslinked and crosslinked NGs did not show significant differences in their in vivo fate, despite the slightly higher size and presumably decreased deformability of the crosslinked nanogels (Figure 7C, 7F). All together, these results demonstrate that the HA and Hep NGs exhibit the same in vivo

behaviour as the native GAGs despite their modification with alkene groups for thiol-ene coupling reactions. Notably, the selective accumulation of Hep NGs in the tumor site make them very promising as nanocarriers for cancer diagnosis and treatment.

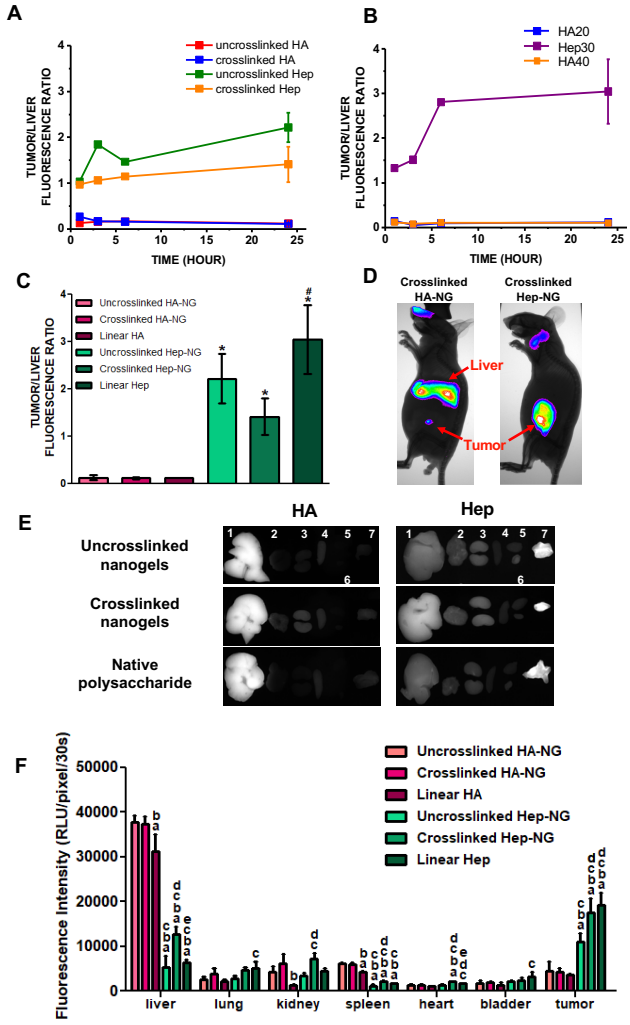

Figure 7. *In vivo* biodistribution of Hep- and HA-NGs in Ehrlich solid tumor-bearing mice. Fluorescence intensity ratio of the excised tumor to liver at 1 h, 3 h, 6 h (n= 1) and 24 h (n = 3) post-injection of Hep- and HA-NGs (A), and of native Hep and HA (B). C) Fluorescence intensity ratio of the excised tumor-to-liver at 24 h post-injection of Hep- and HA-NGs as well as of native Hep and HA (n = 3); error bars represent standard deviations (SD). One-way ANOVA followed by Tukey post hoc test. *# P < 0.05. *Compared to HA (native polysaccharide and nanogels). #Compared to crosslinked Hep-NG. D) *In vivo* fluorescence images of the tumor-bearing mice after intravenous injection crosslinked HA-NGs and Hep-NGs. E) *Ex vivo* fluorescence images of main organs and tumors retrieved from the tumor-bearing mice at 24 h post-injection of NGs and of the native polysaccharides: (1) liver; (2) lung; (3;3') kidney; (4) spleen; (5) heart; (6) bladder; (7) tumor. F) *Ex vivo* fluorescence intensity of main organs at 24 h post-administration of uncrosslinked and crosslinked HA- as well as Hep-NGs and native polysaccharides (HA and Hep) (n = 3). The results were expressed as mean ± SD. One-way ANOVA followed by Tukey post hoc test: [a]Compared to uncrosslinked HA-NG; [b]compared to crosslinked HA-NG; [c]compared to linear HA; [d]compared to uncrosslinked Hep-NG; [e]compared to crosslinked Hep-NG.

Conclusion

In this study, novel biocompatible and biodegradable nanogels based on heparosan were developed by modification of the polysaccharide backbone with a thermoresponsive copolymer, poly(DEGMA-co-BMA), properly designed to obtain stable nanogels at room temperature. The versatile synthetic route to nanogels also allowed their further shell-crosslinking to further store the nanogels at low temperature. After intravenous administration in tumor-bearing mice, both un-crosslinked and crosslinked Hep NGs were able to accumulate in the tumor at a much higher level than their counterparts based on HA. Importantly, the well-defined properties of both Hep and HA NGs families in terms of chemical structure (except the hydrophilic outer-shell), size and morphology allowed to reliably assess the effect of the shell-forming glycosaminoglycan on their in vivo biodistribution. These results thus showed that Hep NGs provide an exciting new class of drug delivery platform for anticancer therapy. To the best of our knowledge, our study provides the first analysis of the in vivo behavior of self-assembled nanoparticles based on Hep, demonstrating significant differences compared to HA-based self-assembled nanoparticles. Regarding the effect of shell-crosslinking on in vivo biodistribution, higher accumulation levels in most of organs, especially in liver and tumor, were observed for the crosslinked Hep NGs compared to the un-crosslinked ones, 24 h after administration. At this stage, it is difficult to explain these results as the un-crosslinked and crosslinked NGs are different not only in size but also in shell stiffness/deformability. So far, the impact of nanoparticles flexibility/stiffness on their function has been very little explored, and the potential benefits of tuning nanoparticle elasticity are not clear. [23-25] Based on these considerations, these Hep NGs represent an attractive platform to investigate the impact of design parameters such as shell crosslinking, incorporation of combination regimens as well as inorganic nanoparticles (magnetic nanoparticles, gold nanoparticles) in order to more optimally exploit the biocompatibility and the beneficial distribution of these novel nanocarriers.

Conflicts of interest

There are no conflicts to declare.

Acknowledgements

The authors are grateful to the "Conselho Nacional de Desenvolvimento Científico e Tecnológico- Conselho Nacional de Desenvolvimento Científico e Tecnológico (CNPq)" for financial support to this work. M.R. gratefully acknowledges the Ministère de l'Enseignement Supérieur, de la Recherche et de l'Innovation (MESRI) for her doctoral training grant. This work was also partly supported by the "Agence Nationale de la Recherche" in the framework of the Glyco@Alps project of the "Investissements d'avenir" program (ANR-15-IDEX-02), and through grants from the Capacitação de Aperfeiçoamento de Pessoal de Nível Superior (CAPES) and Financiadora de Estudos e Projetos (FINEP). The authors thank Francine Roussel-Dherbey at Grenoble INP-CMTC for her help with SEM observations; the

NMR platform of ICMG (FR2607) for its support; B. Priem for valuable discussions.

Notes and references

1. A. Debele Tilahun, L. Mekuria Shewaye and H.-C. Tsai, *Mater Sci Eng C Mater Biol Appl*, 2016, **68**, 964-981.
2. Y. Li, D. Maciel, J. Rodrigues, X. Shi and H. Tomas, *Chem. Rev.*, 2015, **115**, 8564-8608.
3. G. Soni and S. Yadav Khushwant, *Saudi Pharm J*, 2016, **24**, 133-139.
4. H.-Q. Wu and C.-C. Wang, *Langmuir*, 2016, **32**, 6211-6225.
5. M. M. Yallapu, M. Jaggi and S. C. Chauhan, *Drug Discovery Today*, 2011, **16**, 457-463.
6. M. Swierczewska, H. S. Han, K. Kim, J. H. Park and S. Lee, *Adv. Drug Delivery Rev.*, 2016, **99**, 70-84.
7. A. Cadete and M. J. Alonso, *Nanomedicine*, 2016, **11**, 2341-2357.
8. A. M. Carvalho, R. Teixeira, R. Novoa-Carballal, R. A. Pires, R. L. Reis and I. Pashkuleva, *Biomacromolecules*, 2018, **19**, 2991-2999.
9. F. Dosio, S. Arpicco, B. Stella and E. Fattal, *Adv. Drug Delivery Rev.*, 2016, **97**, 204-236.
10. J. Jing, D. Alaimo, E. De Vlieghere, C. Jerome, O. De Wever, B. G. De Geest and R. Auzély-Velty, *J. Mater. Chem. B*, 2013, **1**, 3883-3887.
11. M. Liu, H. Du, A. R. Khan, J. Ji, A. Yu and G. Zhai, *Carbohydr. Polym.*, 2018, **184**, 82-93.
12. M. Liu, H. Du and G. Zhai, *Colloids Surf., B*, 2016, **146**, 235-244.
13. M. Liu, A. R. Khan, J. Ji, G. Lin, X. Zhao and G. Zhai, *J. Controlled Release*, 2018, **290**, 150-164.
14. Y.-S. Liu, C.-C. Chiu, H.-Y. Chen, S.-H. Chen and L.-F. Wang, *Mol. Pharmaceutics*, 2014, **11**, 1164-1175.
15. O. P. Oommen, C. Duehrkop, B. Nilsson, J. Hilborn and O. P. Varghese, *ACS Appl. Mater. Interfaces*, 2016, **8**, 20614-20624.
16. N. V. Rao, H. Y. Yoon, H. S. Han, H. Ko, S. Son, M. Lee, H. Lee, D.-G. Jo, Y. M. Kang and J. H. Park, *Expert Opin. Drug Delivery*, 2016, **13**, 239-252.
17. E. Auzenne, S. C. Ghosh, M. Khodadadian, B. Rivera, D. Farquhar, R. E. Price, M. Ravoori, V. Kundra, R. S. Freedman and J. Klostergaard, *Neoplasia*, 2007, **9**, 479-486.
18. J. E. Draffin, S. McFarlane, A. Hill, P. G. Johnston and D. J. J. Waugh, *Cancer Res.*, 2004, **64**, 5702-5711.
19. Y. Luo and G. D. Prestwich, *Bioconjugate Chem.*, 1999, **10**, 755-763.
20. H. S. S. Qhattal and X. Liu, *Mol. Pharmaceutics*, 2011, **8**, 1233-1246.
21. E. N. Harris and P. H. Weigel, *Glycobiology*, 2008, **18**, 638-648.
22. E. J. Oh, K. Park, K. S. Kim, J. Kim, J.-A. Yang, J.-H. Kong, M. Y. Lee, A. S. Hoffman and S. K. Hahn, *J. Controlled Release*, 2010, **141**, 2-12.
23. S. B. Fox, J. Fawcett, D. G. Jackson, I. Collins, K. C. Gatter, A. L. Harris, A. Gearing and D. L. Simmons, *Cancer Res.*, 1994, **54**, 4539-4546.
24. S. J. Kennel, T. K. Lankford, L. J. Foote, S. G. Shinpock and C. Stringer, *J Cell Sci*, 1993, **104 (Pt 2)**, 373-382.
25. C. R. Mackay, H. J. Terpe, R. Stauder, W. L. Marston, H. Stark and U. Guenthert, *J. Cell Biol.*, 1994, **124**, 71-82.
26. H. J. Terpe, H. Stark, P. Prehm and U. Guenthert, *Histochemistry*, 1994, **101**, 79-89.
27. D. S. Bhattacharya, D. Svechkarev, J. J. Souchek, T. K. Hill, M. A. Taylor, A. Natarajan and A. M. Mohs, *J. Mater. Chem. B*, 2017, **5**, 8183-8192.
28. T. K. Hill, A. Abdulahad, S. S. Kelkar, F. C. Marini, T. E. Long, J. M. Provenzale and A. M. Mohs, *Bioconjugate Chem.*, 2015, **26**, 294-303.
29. T. K. Hill, S. S. Kelkar, N. E. Wojtynek, J. J. Souchek, W. M. Payne, K. Stumpf, F. C. Marini and A. M. Mohs, *Theranostics*, 2016, **6**, 2314-2328.
30. J.-X. Chen, M. Zhang, W. Liu, G.-Z. Lu and J.-H. Chen, *Carbohydr. Polym.*, 2014, **110**, 135-141.
31. P. L. De Angelis, *Expert Opin. Drug Delivery*, 2015, **12**, 349-352.
32. L. Qiu, X. Shan, M. Long, K. S. Ahmed, L. Zhao, J. Mao, H. Zhang, C. Sun, C. You, G. Lv and J. Chen, *Int. J. Biol. Macromol.*, 2019, **130**, 755-764.
33. C. Sun, X. Li, X. Du and T. Wang, *Int. J. Biol. Macromol.*, 2018, **112**, 65-73.
34. R. P. Garay, R. El-Gewely, J. K. Armstrong, G. Garratty and P. Richette, *Expert Opin. Drug Delivery*, 2012, **9**, 1319-1323.
35. K. Knop, R. Hoogenboom, D. Fischer and U. S. Schubert, *Angew. Chem., Int. Ed.*, 2010, **49**, 6288-6308.
36. J. J. F. Verhoef, J. F. Carpenter, T. J. Anchordoquy and H. Schellekens, *Drug Discovery Today*, 2014, **19**, 1945-1952.
37. Q. Yang and S. K. Lai, *Wiley Interdiscip. Rev. Nanomed. Nanobiotechnol.*, 2015, **7**, 655-677.
38. J.-X. Chen, W. Liu, M. Zhang and J.-H. Chen, *Int. J. Pharm.*, 2014, **473**, 493-500.
39. R. S. Lane, F. M. Haller, A. A. E. Chavaroche, A. Almond and P. L. DeAngelis, *Glycobiology*, 2017, **27**, 1062-1074.
40. J. Jing, A. Fournier, A. Szarpak-Jankowska, M. R. Block and R. Auzély-Velty, *Biomacromolecules*, 2015, **16**, 715-722.
41. J. Mergy, A. Fournier, E. Hachet and R. Auzély-Velty, *J. Polym. Sci., Part A Polym. Chem.*, 2012, **50**, 4019-4028, S4019/4011-S4019/4016.
42. M. D'Este, D. Eglin and M. Alini, *Carbohydr. Polym.*, 2014, **108**, 239-246.
43. T. F. Stefanello, M. R. Panice, T. Ueda-Nakamura, M. H. Sarragiotto, R. Auzély-Velty and C. V. Nakamura, *Antimicrob. Agents Chemother.*, 2014, **58**, 7112-7120, 7110 pp.
44. M. Cesaretti, E. Luppi, F. Maccari and N. Volpi, *Carbohydr. Polym.*, 2003, **54**, 59-61.
45. K. K. Upadhyay, A. K. Mishra, K. Chuttani, A. Kaul, C. Schatz, J.-F. Le Meins, A. Misra and S. Lecommandoux, *Nanomedicine*, 2012, **8**, 71-80.
46. T. F. Stefanello, B. Couturaud, A. Szarpak-Jankowska, D. Fournier, B. Louage, F. P. Garcia, C. V. Nakamura, B. G. De Geest, P. Woisel, B. van der Sanden and R. Auzély-Velty, *Nanoscale*, 2017, **9**, 12150-12162.
47. V. Filipe, A. Hawe and W. Jiskoot, *Pharm. Res.*, 2010, **27**, 796-810.
48. A. Banzato, M. Rondina, L. Melendez-Alafort, E. Zangoni, A. Nadali, D. Renier, G. Moschini, U. Mazzi, P. Zanovello and A. Rosato, *Nucl. Med. Biol.*, 2009, **36**, 525-533.
49. K. Y. Choi, K. H. Min, H. Y. Yoon, K. Kim, J. H. Park, I. C. Kwon, K. Choi and S. Y. Jeong, *Biomaterials*, 2011, **32**, 1880-1889.
50. F. P. Garcia, M. Rippe, M. V. P. Companhoni, T. F. Stefanello, B. Louage, S. Van Herck, L. Sancey, J.-L. Coll, B. G. De Geest, C. Vataru Nakamura and R. Auzély-Velty, *Biomater. Sci.*, 2018, **6**, 1754-1763.
51. S. S. Kelkar, T. K. Hill, F. C. Marini and A. M. Mohs, *Acta Biomater.*, 2016, **36**, 112-121.

152. T. Lin, A. Yuan, X. Zhao, H. Lian, J. Zhuang, W. Chen, Q. Zhang, G. Liu, S. Zhang, W. Chen, W. Cao, C. Zhang, J. Wu, Y. Hu and H. Guo, *Acta Biomater.*, 2017, **53**, 427-438.
253. S. R. Datir, M. Das, R. P. Singh and S. Jain, *Bioconjugate Chem.*, 2012, **23**, 2201-2213.
354. A. K. Yadav, A. Agarwal, G. Rai, P. Mishra, S. Jain, A. K. Mishra, H. Agrawal and G. P. Agrawal, *Drug Delivery*, 2010, **17**, 561-572.
455. A. K. Yadav, P. Mishra, A. K. Mishra, P. Mishra, S. Jain and G. P. Agrawal, *Nanomedicine*, 2007, **3**, 246-257.
556. E. N. Harris, J. A. Weigel and P. H. Weigel, *J. Biol. Chem.*, 2008, **283**, 17341-17350.
657. M.-N. Courel, C. Maingonnat, P. Bertrand, C. Chauzy, F. Smadja-Joffe and B. Delpech, *In Vivo*, 2004, **18**, 181-187.
758. J. R. E. Fraser, L. E. Appelgren and T. C. Laurent, *Cell Tissue Res.*, 1983, **233**, 285-293.
859. S. Gustafson and T. Bjorkman, *Glycoconjugate J.*, 1997, **14**, 561-568.
960. P. L. De Angelis, *U.S. patent #20100036001*, 2010.